

Supporting Information for: Electric Field Tunable Ultrafast Interlayer Charge Transfer in Graphene/ WS_2 Heterostructure[†]

Yuxiang Liu,[‡] Jin Zhang,^{*,¶} Sheng Meng,[§] ChiYung Yam,^{*,||,⊥} and Thomas
Frauenheim^{*,‡,||,⊥}

[‡]*Bremen Center for Computational Materials Science, University of Bremen, Am Fallturm
1, 28359 Bremen, Germany*

[¶]*Max Planck Institute for the Structure and Dynamics of Matter, Center for Free Electron
Laser Science, 22761 Hamburg, Germany*

[§]*Beijing National Laboratory for Condensed Matter Physics and Institute of Physics,
Chinese Academy of Sciences, 100190 Beijing, China*

^{||}*Beijing Computational Science Research Center, Haidian District, Beijing, 100193, China*

[⊥]*Shenzhen JL Computational Science and Applied Research Institute, Shenzhen, 518109,
China*

E-mail: jin.zhang@mpsd.mpg.de; yamcy@csrc.ac.cn; thomas.frauenheim@bccms.uni-bremen.de

[†]A footnote for the title

Nonadiabatic Molecular Dynamics with Real-Time Time-Dependent Density Functional Theory

The time-dependent Schrödinger equation for coupled electron-ion systems can be formally written as

$$i\hbar \frac{\partial \Psi(\mathbf{r}, \mathbf{R}, t)}{\partial t} = \hat{H}_{tot}(\mathbf{r}, \mathbf{R}, t) \Psi(\mathbf{r}, \mathbf{R}, t) \quad (\text{S1})$$

where Ψ is the many-body wavefunction, $\mathbf{R} = (\mathbf{R}_1, \mathbf{R}_2, \dots, \mathbf{R}_N)$ is the collective vector of the N ionic positions and $\mathbf{r} = (\mathbf{r}_1, \mathbf{r}_2, \dots, \mathbf{r}_n)$ is the collective vector for n electronic positions. \hat{H}_{tot} is the time-dependent total Hamiltonian given by

$$\begin{aligned} \hat{H}_{tot}(\mathbf{r}, \mathbf{R}, t) = & - \sum_i \frac{\hbar^2}{2m} \nabla_i^2 - \sum_I \frac{\hbar^2}{2M_I} \nabla_I^2 + \frac{1}{2} \sum_{i \neq j} \frac{e^2}{|\mathbf{r}_i - \mathbf{r}_j|} \\ & + \frac{1}{2} \sum_{I \neq J} \frac{Z_I Z_J}{|\mathbf{R}_I - \mathbf{R}_J|} - \sum_{i,I} \frac{e Z_I}{|\mathbf{r}_i - \mathbf{R}_I|} + \hat{V}_{ext}(\mathbf{r}, \mathbf{R}, t) \end{aligned} \quad (\text{S2})$$

Here, m and e denote the electronic mass and charge, M_I and Z_I are the mass and charge of I th ion, and \hat{V}_{ext} is the external potential. According to Runge-Gross theorem,¹ the external potential for electrons and ions can be determined by their densities, ρ and ρ_I , respectively. The following electronic and ionic time-dependent Kohn-Sham equation (TDKS) can be expressed as

$$i\hbar \frac{\partial \phi_i(\mathbf{r}, t)}{\partial t} = \left[-\frac{\hbar^2}{2m} \nabla_i^2 + \hat{v}_s[\rho](\mathbf{r}, t) \right] \phi_i(\mathbf{r}, t) \quad (\text{S3})$$

$$i\hbar \frac{\partial \chi_I(\mathbf{R}_I, t)}{\partial t} = \left[-\frac{\hbar^2}{2m} \nabla_I^2 + \hat{V}_S^I[\rho_I](\mathbf{R}_I, t) \right] \chi_I(\mathbf{R}_I, t) \quad (\text{S4})$$

where ϕ and χ are the single-particle electronic and nuclear wavefunctions, respectively. The densities are given by $\rho(\mathbf{r}, t) = \sum_i |\phi_i(\mathbf{r}, t)|^2$ and $\rho_I(\mathbf{R}_I, t) = |\chi_I(\mathbf{R}_I, t)|^2$.

The single particle external potential $\hat{v}_s[\rho]$ and $\hat{V}_S^I[\rho_I]$ are as follows:

$$\hat{v}_s[\rho](\mathbf{r}, t) = \int \frac{\rho(\mathbf{r}', t)}{|\mathbf{r} - \mathbf{r}'|} d\mathbf{r}' - \sum_I \int \frac{Z_I \rho_I(\mathbf{r}, t)}{|\mathbf{r} - \mathbf{R}_I|} d\mathbf{R}_I + \hat{v}_{ext}(\mathbf{r}, t) + \hat{v}_{xc}[\rho](\mathbf{r}, t) \quad (\text{S5})$$

$$\begin{aligned} \hat{V}_S^I[\rho_I](\mathbf{R}_I, t) = & Z_I \sum_J \int \frac{Z_J \rho_J(\mathbf{R}_J, t)}{|\mathbf{R}_I - \mathbf{R}_J|} d\mathbf{R}_J - Z_I \int \frac{\rho(\mathbf{r}, t)}{|\mathbf{R}_I - \mathbf{r}|} d\mathbf{r} \\ & + \hat{V}_{ext}^I(\mathbf{R}_I, t) + \hat{V}_{xc}[\rho_I](\mathbf{R}_I, t) \end{aligned} \quad (\text{S6})$$

As the nuclei are much heavier than electrons, we invoke the Ehrenfest dynamics theorem for the nuclear TDKS equation, in which ionic motion follows Newton's second law:

$$M_I \frac{d^2 \mathbf{R}_I(t)}{dt^2} = -\nabla_I \left[\sum_{I \neq J} \frac{Z_I Z_J}{|\mathbf{R}_I - \mathbf{R}_J|} - Z_I \int \frac{\rho(\mathbf{r}, t)}{|\mathbf{R}_I - \mathbf{r}|} d\mathbf{r} + \hat{V}_{ext}^I(\mathbf{R}_I, t) \right] \quad (\text{S7})$$

Note that we ignore the ion-ion exchange-correlation functional and assume a sharp ionic density distribution $\rho_I(\mathbf{R}, t) = \delta(\mathbf{R} - \mathbf{R}_I(t))$. On the other hand, the electronic motion follows the TDKS equations, where

$$\begin{aligned} i\hbar \frac{\partial \phi_i(\mathbf{r}, t)}{\partial t} = & \left[-\frac{\hbar^2}{2m} \nabla_i^2 + \int \frac{\rho(\mathbf{r}', t)}{|\mathbf{r} - \mathbf{r}'|} d\mathbf{r}' - \sum_I \frac{Z_I}{|\mathbf{r} - \mathbf{R}_I|} \right. \\ & \left. + \hat{v}_{ext}(\mathbf{r}, t) + \hat{v}_{xc}[\rho](\mathbf{r}, t) \right] \phi_i(\mathbf{r}, t) \end{aligned} \quad (\text{S8})$$

Eq. S7 and Eq. S8 describe the time-dependent propagation of a coupled electron-nuclear system. Within TDDFT, the electronic subsystem is described quantum mechanically, while the nuclear subsystem evolves along classical Newton's trajectories with the forces obtained from an averaged potential energy based on the Ehrenfest theorem.

Computational Details

First-principles calculations of graphene/WS₂ heterostructure are performed with linear combination of atomic orbital methods implemented in SIESTA,² using PBE exchange-correlation functional.^{3,4} Troullier-Martins norm-conserving pseudopotentials⁵ are employed to describe the core electrons. The orthogonal 5×5 graphene/ 4×4 WS₂ supercell is fully relaxed (atomic positions and lattice vectors) until the residual forces are less than 5×10^{-3} eV/Å and the total energy variation is less than 10^{-6} eV with the vdW vdw-DF2 functional.⁶ This results lattice parameter $a = 12.4325$ Å and $b = 21.5241$ Å, corresponding to 0.6% stretch of graphene and 1.7% compression of WS₂. The Brillouin Zone is sampled by $5 \times 5 \times 1$ k-mesh grid with a 250 Ry energy cutoff for the orthogonal supercell to obtain electronic band structures. A 30 Å vacuum layer is employed to avoid the interactions between repeated images.

The electron and nuclear dynamics are simulated within the time-dependent ab initio package (TDAP).⁷ Similarly, Troullier-Martins norm-conserving pseudopotentials⁵ and PBE exchange-correlation functional^{3,4} are used for core electrons. The supercell is sampled at Γ point. With Γ -point approximation, some of graphene states within the band gap of WS₂ are ignored, this may slow down the longer time-scale carrier recombination in graphene but have minor effects on the ultrafast interlayer charge transfer process. For molecular dynamics, we use NVE ensemble with a time step of 0.02419 fs. Initial ion velocities are obtained by the equilibrium Boltzmann-Maxwell distribution at a given temperature 300 K. Spin-orbit coupling (SOC) is ignored in the simulations. SOC results in two main effects. First, a band gap is opened at Dirac point due to symmetry breaking of graphene pseudospin. Second, the spin degeneracies of valence and conduction band at Dirac point are lifted and give rise to four distinct bands.⁸ Since the changes in the electronic band structure are on the order of meV, the effects on the short time carrier dynamics and couplings between carrier states are insignificant. Therefore, it is expected that ignoring SOC would not affect the overall interlayer dynamics.

Density of States

Figure S1 shows the density of states (DOS) of graphene/WS₂ heterostructure applied with different external electric fields, varying from -0.3 V/Å to +0.3 V/Å. The density of acceptor states for photoexcited electron and hole are similar when no electric field is applied. Thus, it is expected the availability of acceptor states for electron and hole transfer should be similar. The more efficient interlayer hole transfer is rather attributed to the couplings between states on the two layer. In the case of applied fields, it can be seen that negative electric field significantly increases the density of acceptor states for hole transfer, which is 10 times more than that for electron transfer. Meanwhile, positive electric field has the same effect on the density of acceptor states for electron transfer.

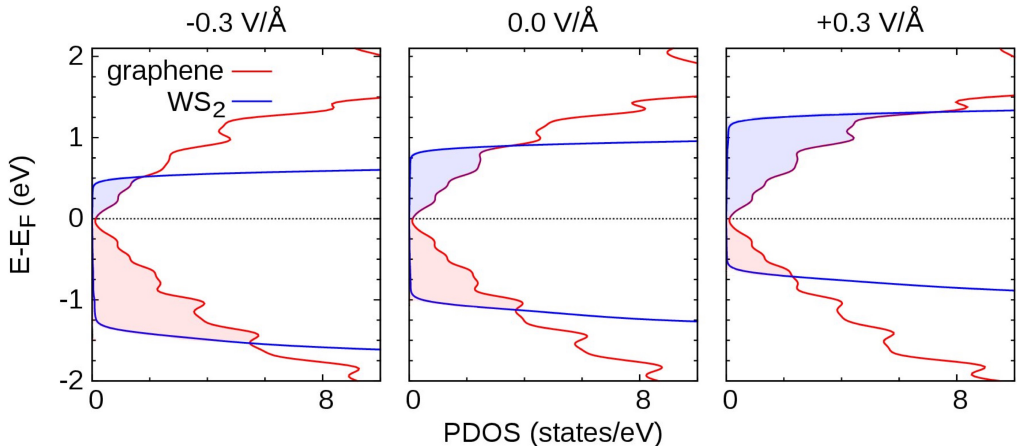


Figure S1: The DOS of graphene/WS₂ heterostructure with external electric fields, varying from -0.3 V/Å to +0.3 V/Å. The density of acceptor states on graphene for photoexcited electron and hole are illustrated by blue and red areas, respectively.

The coupling between donor and acceptor states

We define the coupling between donor and acceptor states by projecting the time-dependent density matrix P onto initial eigenstates,

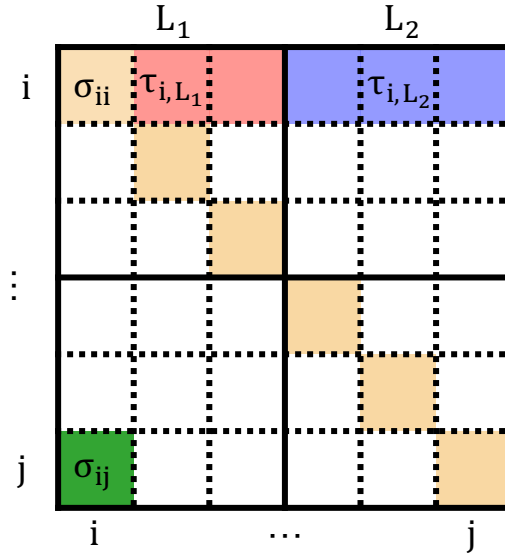


Figure S2: Illustration of the coupling matrix. σ is divided into sub-blocks according to different layers (solid lines), and the sub-blocks are further divided into eigenstates within the layer (dashed lines). The diagonal element σ_{ii} , shaded by yellow, represents the occupation of state i . The off-diagonal element σ_{ij} , shaded by green, represents the coupling between states i and j . Summing up all the off-diagonal elements within the layer L_1 (red shaded area) or L_2 (blue shaded area) gives the coupling between state i and all states on layer L_1 or L_2 , denoted by τ_{i,L_1} or τ_{i,L_2} respectively.

$$\sigma_{ij}(t) = \sum_{\mu\nu\kappa\lambda} (c_{\mu i}(0)S_{\kappa\mu})^* P_{\kappa\lambda}(t) S_{\lambda\nu} c_{\nu j}(0) \quad (\text{S9})$$

where c is the molecular orbital coefficient and $\mu, \nu, \kappa, \lambda$ are atomic orbitals. The overlap matrix S and single-electron density matrix P are in non-orthogonal atomic basis representation. The summation in the above equation runs over all atomic orbitals. i and j are the eigenstates at $t=0$.

As shown in Figure S2, σ is divided into sub-blocks labelled by the layer number L , and each sub-block contains all the eigenstates localized in the layer. The diagonal element σ_{ii} (yellow block) represents the occupation of the state i , and the off-diagonal element σ_{ij} (green block) represents the coupling between states i and j . The coupling between i and states on the layer of interest is then obtained by summing over all the off-diagonal elements within L ,

$$\tau_{i,L}(t) = \sum_{j \neq i, j \in L} |\sigma_{ij}(t)| \quad (\text{S10})$$

for example, the red block represents the coupling between state i and all states on layer L_1 , denoted by τ_{i,L_1} . Similarly, τ_{i,L_2} (blue block) is the coupling between state i and all states on layer L_2 . In this work, L_1 and L_2 represent graphene and WS_2 , respectively.

Excitation dynamics of graphene/ WS_2 heterostructure with frozen atoms

In the case of graphene/ WS_2 heterostructure with all frozen atoms, the Fourier transforms (FTs) of $n_{e/h}(t)$, $\epsilon_{e/h}(t)$ and $\tau_{e/h,G}(t)$ are presented in Figure S3. Both photoexcited hole and electron dynamics show characteristic frequencies at $\sim 657 \text{ cm}^{-1}$ and $\sim 1100 \text{ cm}^{-1}$, which are close to the frequencies of $\sim 620 \text{ cm}^{-1}$ and $\sim 1067 \text{ cm}^{-1}$ obtained with moving atoms. Further investigation shows that these two frequencies can also be observed in the scenario

when only WS₂ or graphene layer is clamped (Figure S5, grey shaded areas). This result demonstrates that the above oscillations are not related to the atom vibration, originating from the collective motion of carriers.⁹

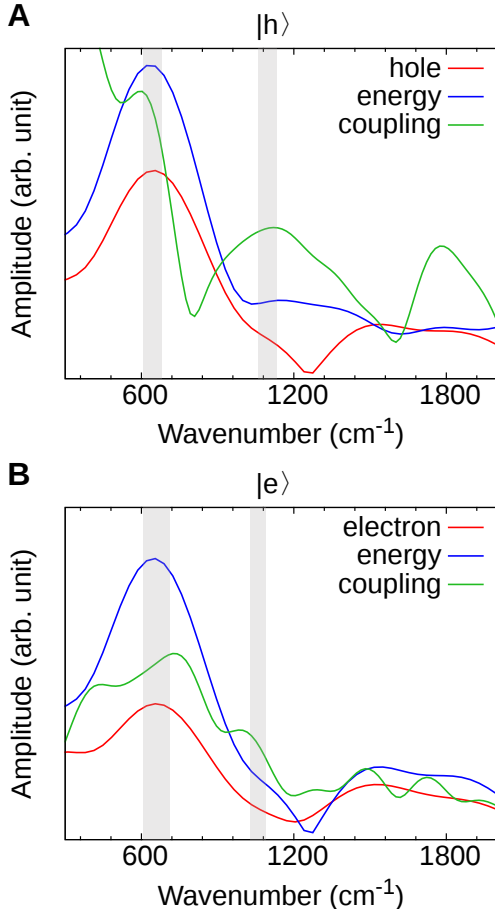


Figure S3: Comparison of FTs of photoexcited (A) hole and (B) electron transferred to graphene $n_{e/h}(t)$, their corresponding energies $\epsilon_{e/h}(t)$ and the coupling to electronic states of graphene layer $\tau_{e/h,G}(t)$ with all frozen atoms. Red, blue and green curves correspond to the FTs of $n_{e/h}(t)$, $\epsilon_{e/h}(t)$ and $\tau_{e/h,G}(t)$, respectively. The grey shaded areas represent the frequencies associated with the collective motion of carriers.

To further confirm the relationship between nuclear vibrational modes and interlayer charge transfer process, photoexcited carrier localization on graphene and WS₂ layers with all frozen atoms are simulated, as shown in Figure S4. As mentioned in manuscript, the coupling between excited carriers and states of graphene plays a key role in the carrier interlayer dynamics. Stronger coupling between photoexcited hole and graphene states drives

hole filling and emptying periodically the nearby graphene states. Meanwhile, a majority of photoexcited electron relaxes to WS_2 states of low energy and resides on WS_2 layer due to its stronger coupling to WS_2 states.

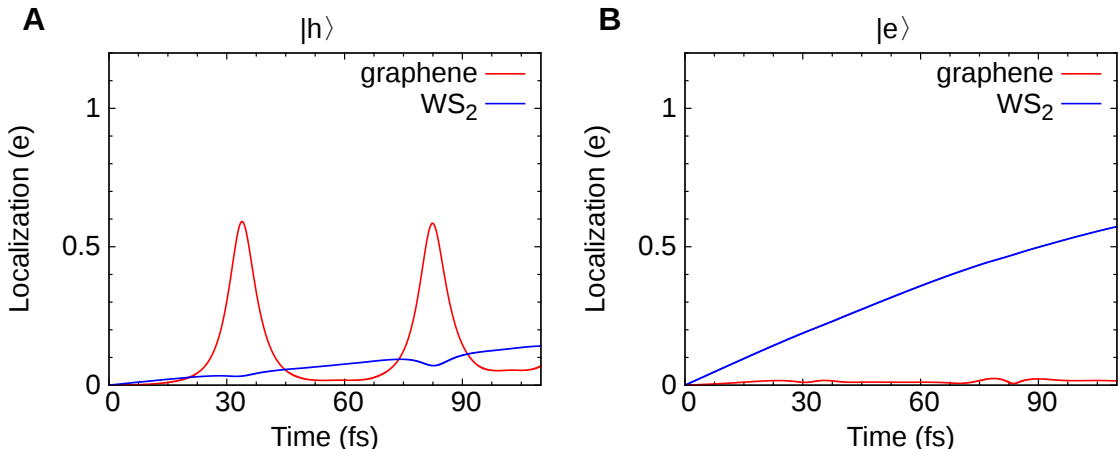


Figure S4: The time evolution of photoexcited (A) hole and (B) electron localization on graphene and WS_2 with all frozen atoms.

The excitation dynamics with clamped graphene and WS_2 layers in frequency domain is presented in Figure S5. As discussed in the manuscript, the vibrational mode G^{10} of graphene is associated with photoexcited hole and electron interlayer transfer process. When atoms in WS_2 layer are clamped, photoexcited hole and electron dynamics indeed exhibit characteristic oscillation of the C=C stretching mode G, shaded by red areas in Figure S5A. In contrast, the out-of-plane vibration A_{1g}^{11} in WS_2 only contributes to the electron interlayer transfer. As showed in Figure S5B, A_{1g} -mode (shaded by red area) can only be observed in electron dynamics when atoms in graphene are fixed. These results further demonstrate that nuclear vibrations in graphene are associated with both hole and electron interlayer transfer while nuclear vibrations in WS_2 are only coupled to electron transfer.

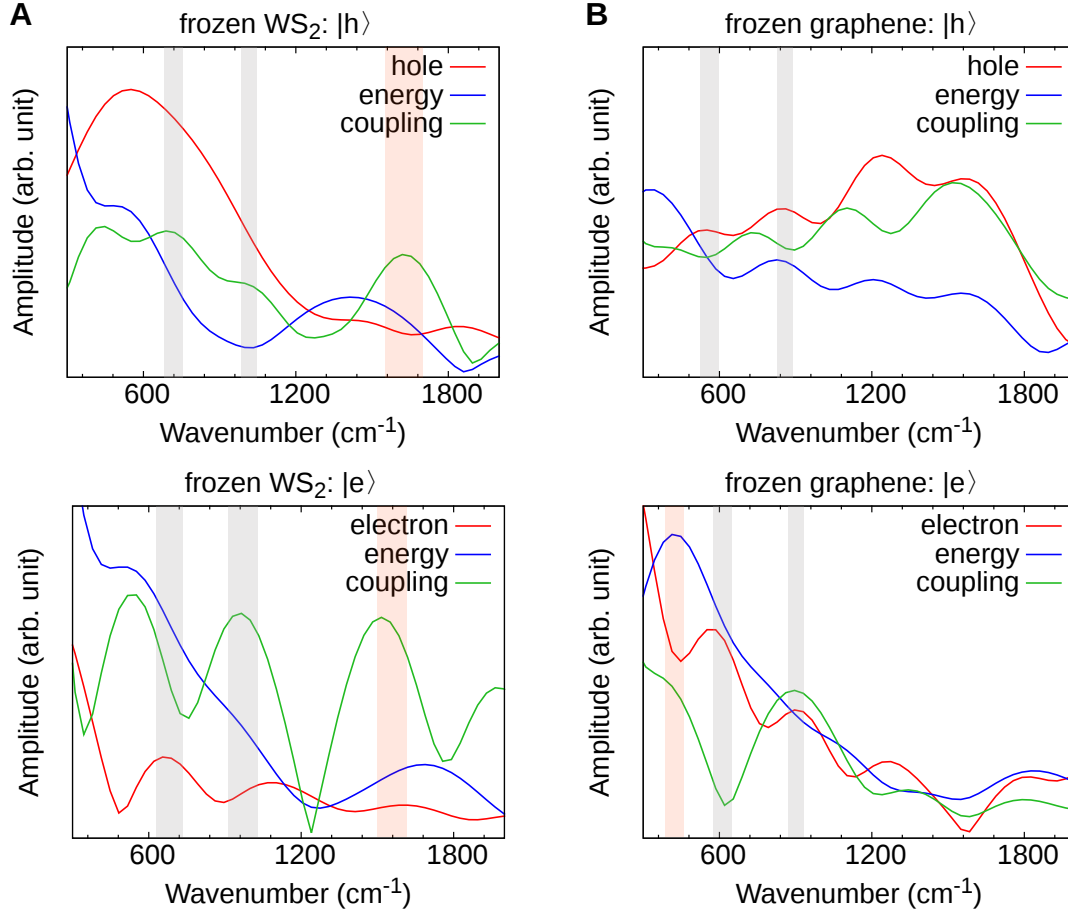


Figure S5: Comparison of FTs of photoexcited hole and electron transfer to graphene $n_{e/h}(t)$, their corresponding energies $\epsilon_{e/h}(t)$ and the coupling to electronic states of graphene layer $\tau_{e/h,G}(t)$ with (A) frozen WS_2 layer and (B) frozen graphene layer. Red, blue and green curves correspond to the FTs of $n_{e/h}(t)$, $\epsilon_{e/h}(t)$ and $\tau_{e/h,G}(t)$, respectively. The red shaded areas represent the frequencies associated with ionic vibrations, and grey shaded areas represent the frequencies associated with the collective motion of carriers.

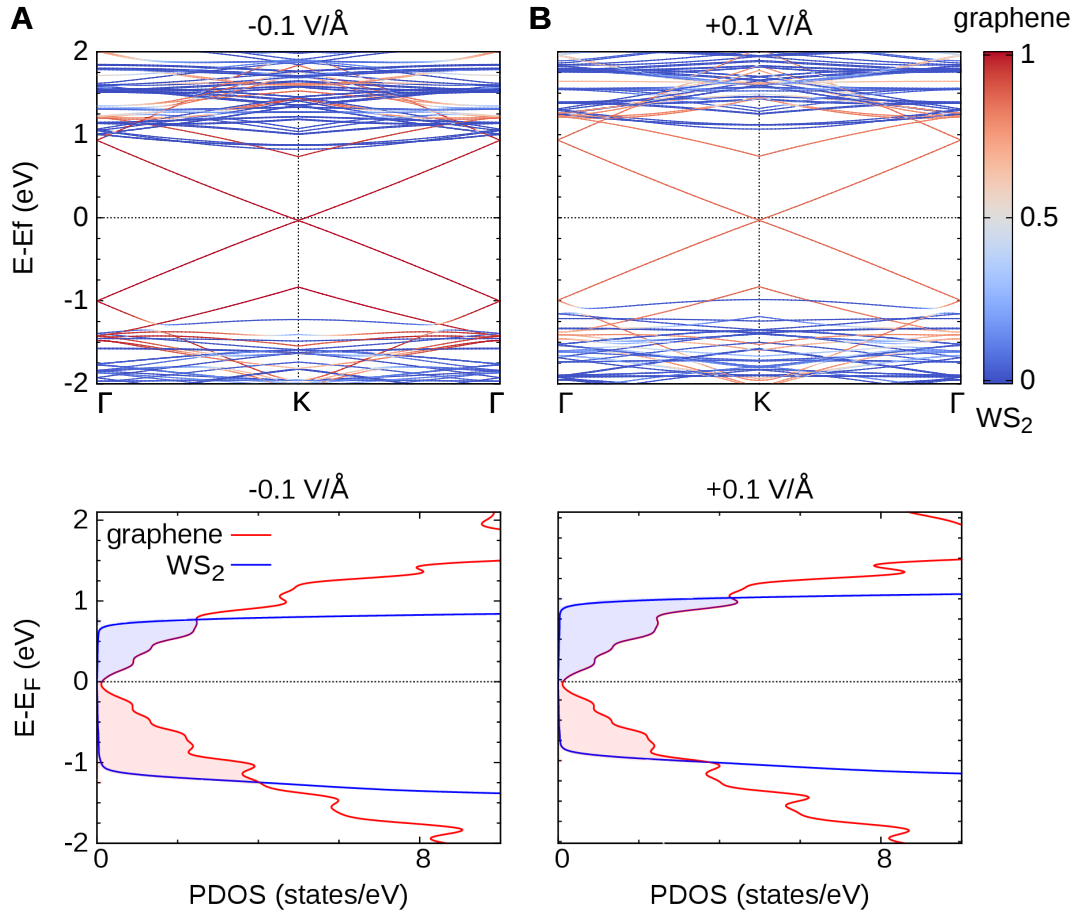


Figure S6: The band structures and DOS of graphene/WS₂ heterostructure with different applied electric fields, varying from (A) -0.1 V/\AA to (B) $+0.1 \text{ V/\AA}$. Fermi energy is set to zero. Same color map as Figure 1D is employed to show the charge localization. The density of acceptor states on graphene for photoexcited electron and hole are illustrated by blue and red areas, respectively.

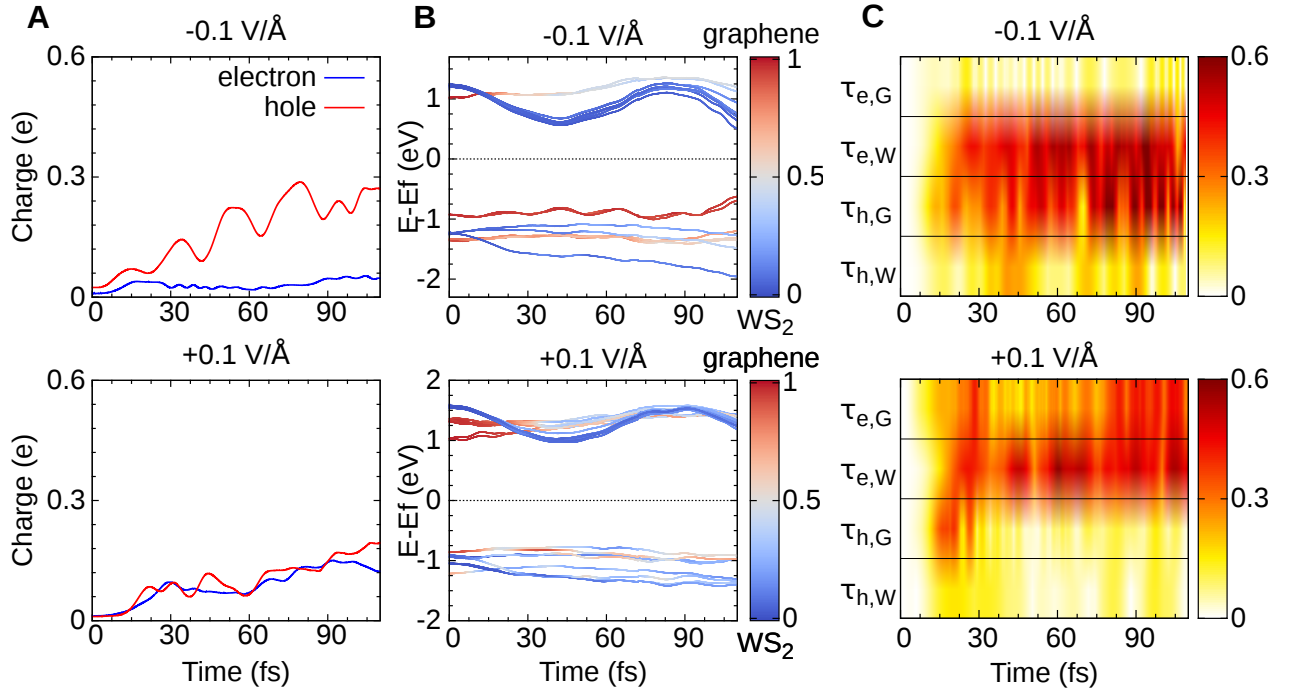


Figure S7: Excitation dynamics of graphene/WS₂ heterostructure with external electric fields varying from -0.1 V/Å to +0.1 V/Å. (A) Amount of photoexcited electron and hole transferred from WS₂ to graphene. (B) Time evolution of the energy levels $\epsilon(t)$. Same color map as the Figure 1D is employed to show the charge localization. (C) Time evolution of the couplings, $\tau_{e,G}(t)$, $\tau_{e,W}(t)$, $\tau_{h,G}(t)$ and $\tau_{h,W}(t)$. The color indicates the strength of the coupling between photoexcited carriers and acceptor states.

Excitation dynamics of graphene/WS₂ heterostructure applied with electric fields

Applied with $-0.1\text{V}/\text{\AA}$ and $+0.1\text{V}/\text{\AA}$ electric fields, electronic structures of graphene/WS₂ heterostructure exhibit the similar response as that applied with $-0.3\text{V}/\text{\AA}$ and $+0.3\text{V}/\text{\AA}$ electric fields. As shown in Figure S6A, $-0.1\text{V}/\text{\AA}$ electric field downshifts the WS₂ states, which increases acceptor states for hole transfer and simultaneously suppresses electron transfer due to the decrease of available states. On the contrary, $+0.1\text{V}/\text{\AA}$ electric field upshifts the WS₂ states, and thus accelerates electron transfer but impedes hole transfer. The time evolution of $n_{e/h}(t)$, $\epsilon_{e/h}(t)$ and $\tau_{e/h,L}(t)$ are presented in Figure S7 to further demonstrate the above findings. For the case of $+0.1\text{V}/\text{\AA}$ electric field, it is found that some of the states are delocalized over both graphene and WS₂ layers. Taking into account the delocalization effect, Eq. S10 is modified by including a weight factor f_j^L : $\tau_{i,L}(t) = \sum_{j \neq i, j \in L} f_j^L |\sigma_{ij}(t)|$. f_j^L corresponds to the fraction of the state j that are localized on layer L . With an applied electric field of $-0.1\text{V}/\text{\AA}$, $\tau_{h,G}(t)$ is enhanced, and thus hole transfer is significantly accelerated. On the other hand, $+0.1\text{V}/\text{\AA}$ electric field induces a stronger $\tau_{e,G}(t)$ which facilitates the electron interlayer dynamics. Therefore, the coupling between donor and acceptor states indeed can be controlled by external electric fields, and thus achieve the manipulation of charge transfer rate at heterointerfaces.

References

- (1) Runge, E.; Gross, E. K. Density-Functional Theory for Time-dependent Systems. *Phys. Rev. Lett.* **1984**, *52*, 997.
- (2) Soler, J. M.; Artacho, E.; Gale, J. D.; García, A.; Junquera, J.; Ordejón, P.; Sánchez-Portal, D. The SIESTA Method for Ab Initio Order-N Materials Simulation. *J. Phys. Condens. Matter* **2002**, *14*, 2745.

- (3) Blöchl, P. E. Projector Augmented-Wave Method. *Phys. Rev. B* **1994**, *50*, 17953.
- (4) Perdew, J. P.; Burke, K.; Ernzerhof, M. Generalized Gradient Approximation Made Simple. *Phys. Rev. Lett.* **1996**, *77*, 3865.
- (5) Troullier, N.; Martins, J. L. Efficient Pseudopotentials for Plane-Wave Calculations. *Phys. Rev. B* **1991**, *43*, 1993.
- (6) Lee, K.; Murray, É. D.; Kong, L.; Lundqvist, B. I.; Langreth, D. C. Higher-Accuracy Van Der Waals Density Functional. *Phys. Rev. B* **2010**, *82*, 081101.
- (7) Meng, S.; Kaxiras, E. Real-time, Local Basis-Set Implementation of Time-Dependent Density Functional Theory for Excited State Dynamics Simulations. *J. Chem. Phys.* **2008**, *129*, 054110.
- (8) Yang, B.; Tu, M.-F.; Kim, J.; Wu, Y.; Wang, H.; Alicea, J.; Wu, R.; Bockrath, M.; Shi, J. Tunable Spin–Orbit Coupling and Symmetry-Protected Edge States in Graphene/WS₂. *2D Mater.* **2016**, *3*, 031012.
- (9) Wang, H.; Bang, J.; Sun, Y.; Liang, L.; West, D.; Meunier, V.; Zhang, S. The Role of Collective Motion in the Ultrafast Charge Transfer in Van Der Waals Heterostructures. *Nat. comm.* **2016**, *7*, 1–9.
- (10) Dresselhaus, M. S.; Jorio, A.; Hofmann, M.; Dresselhaus, G.; Saito, R. Perspectives on Carbon Nanotubes and Graphene Raman Spectroscopy. *Nano Lett.* **2010**, *10*, 751–758.
- (11) Zhao, W.; Ghorannevis, Z.; Amara, K. K.; Pang, J. R.; Toh, M.; Zhang, X.; Kloc, C.; Tan, P. H.; Eda, G. Lattice Dynamics in Mono- and Few-Layer Sheets of WS₂ and WSe₂. *Nanoscale* **2013**, *5*, 9677–9683.